31st Congress of the International Council of the Aeronautical Sciences

Belo Horizonte, Brazil; September 09-14, 2018

INFLUENCE OF AIRFRAME STIFFNESS ON THE AERODYNAMIC COEFFICIENTS OF A HIGH ASPECT RATIO WING

Luís A. V. Pelegrineli* , **Felipe F. Liorbano*** , **Henrique O. H. Natori*** , **Ricardo A. Angélico***
University of São Paulo, São Carlos School of Engineering, Department of Aeronautical Engineering*

Keywords: *flexible wings, experimental aerodynamics, aerodynamic coefficients, wind-tunnel tests.*

Abstract

The use of new materials into airframe enabled lighter and more flexible aircraft. The structural flexibility of aerodynamic surfaces can significantly change aircraft performance. In this context, the present article aims to furnish experimental data (lift and drag coefficients) of flexible wings by tests performed at EESC-USP open circuit wind tunnel. The model consists of a rectangular wing with 0.60 m semi-span and aspect ratio of 8.88 with a Clark-Y airfoil with two possible stiffness. The stiffer configuration was adopted as a reference condition. Non-invasive techniques were employed to measure twist angle and the displacement of the wing. For this wing model tested with 20.5 m/s ($Re \approx 191,000$), it was shown that the effects of flexibility on the aerodynamic coefficients considering performance parameters were adverse, especially for high angles of attack, where the aerodynamic loads are higher. Also, the identification of wing displacement and its torsion contributes to a better understanding of the aerodynamic behavior. Wing torsion and displacements measurements are presented for three angles of attack (0°, 6° and 14°). The experimental results presented herein can be used for validation of computational codes on flexible wings.

1 Introduction

With the advent of new materials on aeronautical industry, the shape of modern aircraft components may change during flight due to high structural deflections. For instance, the wings withstand aerodynamic loads which can change their format significantly, especially on airplanes with high aspect ratio wings. Some airplanes, like Boeing 787 [1] and Airbus A380 [2], when under the ultimate-load wing-up bending test, have their wing tips deflected more than 7.5 m. This change in the wing shape plays an important role on the aircraft aerodynamic coefficients and, consequently, on its performance. In such a way, it is important to estimate the losses on the aircraft performance due to these effects. To accomplish this, it is necessary to understand the influence of the geometric nonlinearities of a wing on its aerodynamic coefficients. In this context, some authors investigated experimentally and analytically the aerodynamic behavior of flexible lifting surfaces.

Tang and Dowell [3] performed wind tunnel tests to investigate the effect of bursts on flexible wings with high aspect ratio. Albertani [4] carried out wind tunnel tests in MAVs (Micro Air Vehicles), integrating visual image correlation to measure structural deflections.

Hooker et al. [5] presented a method to predict aeroelastic deformation (twist and bending) via FEM (Finite Element Method) which was validated by wind tunnel tests.

Nguyen and Chaparro [6] presented a coupled aerodynamic-nonlinear finite element model for a wind tunnel model designed to have about 10 % wingtip deflection. This wind tunnel model represents the state of the art of high aspect ratio

wings and was used to validate a real-time adaptive drag optimization control strategy. The description of this wind tunnel model was presented by Vassberg et al. [7] and was motivated by the need for contemporary experimental databases to validate computational fluid dynamics (CFD) applications.

This highlights the importance of experimental aerodynamic data of flexible lifting surfaces. The present article aims to investigate the influence of structural flexibility on the aerodynamic coefficients of a high aspect ratio flexible wing via wind tunnel testing, providing experimental data of flexible wings to validate FSI (Fluid-Structure Interaction) computational codes.

2 Experimental procedure

2.1 Wing model

The model consists of a rectangular wing with 0.60 m semi-span and aspect ratio of 8.88 with a Clark-Y airfoil. The airfoil was selected due to its horizontal lower surface, which facilitates its positioning at the wind tunnel. In addition, as presented by Marchman and Werme [8], the Clark-Y airfoil performs well at low Reynolds numbers ($50,000 \leq Re \leq 200,000$) for wind tunnel tests.

The wing model was designed to allow the change in stiffness by introducing or removing the spars, as shown in Figure 1. This way, the same model can be used for tests with different stiffness levels, diminishing the influence on the results due to causes other than the variable wing curvature and twist in span direction when submitted to aerodynamic load. The model consists of a hexagonal brass spar 5.6 mm width across the flat and a removable 8.0 mm diameter steel bar. For the configuration with higher stiffness, the steel spar is introduced to increase the stiffness of the system. These spars are connected to the aerodynamic balance located at the right wall side of the test section.

The wing ribs are made of epoxy resin and have weight relief holes, which are also used to accommodate the inertial measurement units (IMUs) used to measure the twist angle along the wingspan. In both configurations, the wing deflection is allowed by the introduction of small gaps between the ribs, as shown in Figure 1. Thus, the ribs do not influence the wing stiffness, even when the deflection is high. The wing model in its configuration with two spars is shown in Figure 2.

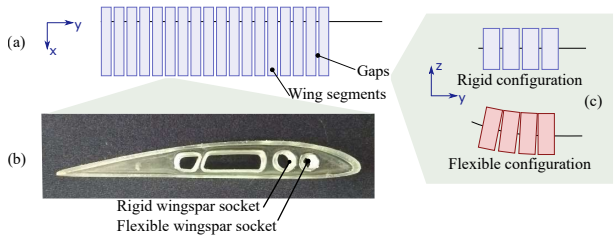

Fig. 1 Wing model: (a) scheme of the wing model; (b) wing segment made of epoxy resin; (c) wing sockets for different spars.

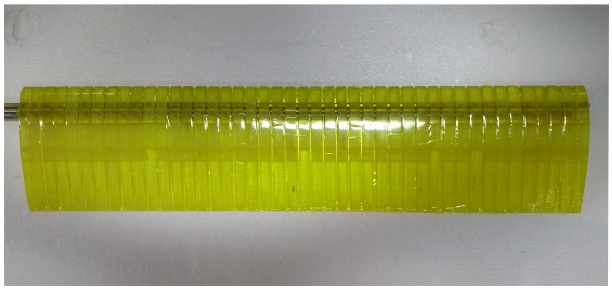

Fig. 2 Wing model with brass and steel spars (rigid configuration).

2.2 Wind tunnel and model instrumentation

The instrumentation used in the experiments was aimed at extracting aerodynamic data, such as the drag and lift coefficients for a wing with different stiffness levels, as well as data related to the rotation of wing sections around the x and y-axes. Besides, the wing was photographed in its y-z plane to obtain data related to its deflection along the z-axis.

Concerning aerodynamic data, an NI-9237 module in conjunction with a National Instruments^{TM} cDAQ-9191 chassis was used to communicate the software LabVIEW with the balance coupled with the wind tunnel. For the dynamic pressure measurement, it was used

a Pitot tube connected to a TSI^{TM} DP-CALC 8705-M-GB micromanometer. For the acquisition of the temperature and the local atmospheric pressure an ITWH-1170 meteorological station of Instrutemp^{TM} was used.

Along the wingspan, IMUs (MPU 6050-GY 521) integrated into an Arduino Mega^{TM} board were arranged in five sections, and thus, the rotation around the x and y-axes of these sections were calculated from measurements of the components of the gravitational acceleration in the x, y and z directions.

For the acquisition of the deflections of the wing in the z-direction, a Canon^{TM} EOS-Rebel T7i camera was used along with a Canon^{TM} EF-S 18-55 mm f/4-5.6 IS STM lens.

The deflection of the wing was computed by post-processing the images acquired throughout the tests. The images obtained are in RGB format. The color of a pixel in an RGB image is the combination of three colors: red (R), green (G) and blue (B). Then, the color of a pixel located at $\mathbf{x} = (x, y)$ is

$$I(\mathbf{x}) = a_r I_r(\mathbf{x}) + a_g I_g(\mathbf{x}) + a_b I_b(\mathbf{x}) \qquad (1)$$

where $I_r(\mathbf{x})$, $I_g(\mathbf{x})$ and $I_b(\mathbf{x})$ are the red, green and blue layers of I; and a_r, a_g, a_b are multipliers.

In the first step, the multipliers were chosen to highlight the region of interest. The green layer had an intensity distribution that highlighted the wing, but the red layer was also required since the walls of the closed test section interfered in the identification of the wing root. Then, a threshold filter based on I_r and I_g binarized the image, giving a new image $\bar{I}(\mathbf{x})$, i.e.

$$\bar{I}(\mathbf{x}) = (I(\mathbf{x}) > a_{T_1} \max(I_g)) \cap (I_g - I_r) > a_{T_2} \qquad (2)$$

where $\max(I_g)$ returns the maximum intensity of I_g and a_{T_1} and a_{T_2} are threshold parameters.

Next, the wing contour was identified and midpoints between the upper and lower bounds were computed. These points were transformed to the aerodynamic coordinate system and the pixels coordinates were converted to millimeters. This conversion factor was obtained by correlating the dimensions of a checkerboard and its respective dimensions in pixels on the plane containing the midpoints. Finally, a cubic curve was used to fit the data.

2.3 Wind tunnel tests

The wind tunnel tests were performed at the Aeronautical Engineering Department of the São Carlos School of Engineering of the University of São Paulo in a blowing type wind tunnel with a closed test section. The experimental procedure was conducted as follows:

1. The wing model was positioned at the wind tunnel and connected to an aerodynamic balance at an angle of attack of -8 degrees.
2. The balance was tared in a wind-off configuration.
3. The wind tunnel was turned on and the aerodynamic forces measurements were taken from the angle of attack range of -8 to 16 degrees for the configuration with lower stiffness. For each angle of attack, the temperature, the dynamic pressure of the flow and the atmospheric pressure were measured.
4. An 8.0 mm steel spar was introduced to the wing model to increase its stiffness.
5. The steps 1 to 3 were repeated for the new wing configuration.

After the aerodynamic forces measurements, the same wing was instrumented with the previously described IMUs along the semi-wing span and the photographic camera was positioned downstream of the wing model to take the pictures used for the deflection measurements. Then, the steps 1 to 5 were repeated for this instrumented wing for both stiffness configurations. This time, for each angle of attack, the IMUs data and a photo was taken for each angle of attack. These data were used to compute wing deflection and twist along the semi-span. All the tests were performed at the same Reynolds number, approximately 191,000.

The results obtained for the aerodynamic forces (lift and drag) and measured dynamic pressure were corrected for the solid blockage, the

wake blockage and the downwash effects. The correction methods used were presented by Pope et al. [9].

3 Results

The airframe stiffness influences the aircraft performance, and it must be quantified to get closer to the real aircraft characteristics. Herein, as mentioned before, its influence is experimentally investigated by the testing of two configurations: rigid (R) and flexible (F). The wing aerodynamic coefficients – lift coefficient vs. angle of attack and lift coefficient vs. drag coefficient – can be seen in Figure 3. For low values of lift coefficient, C_L between -0.25 and 0.25, the stiffer and flexible configurations present almost the same behavior. With the increase of the lift coefficient magnitude, $C_L > 0.25$, the difference between the curves also increases, with the stiffer configuration presenting the higher values. On the other hand, the significant differences for the drag occur for $C_L < 0.6$. The flexible configuration – in comparison with the stiffer one – decreases the aircraft performance in takeoff and landing due to the C_{Lmax} reduction. The reduction of C_{Lmax} was 5.85 % for a Reynolds number about 191,000. Also, for typical climb and cruise lift coefficients, $0.3 < C_L < 0.6$, the flexible configuration shows a higher drag coefficient, leading to a performance reduction in these mission profile phases. For instance, for a C_L equals to 0.4, the drag coefficient difference is 16 %.

For the flexible configuration, the aerodynamic coefficients depend on the dynamic pressure, once the wing shape varies with the airspeed. The wing motion due to the dynamic pressure decomposes into flexion and torsion. The model was built to be flexible only along the axis y, so that, the lift is the driving force of the wing movement. The wing flexion was monitored by the camera and its torsion by the inertial sensors embedded into the wing. The wing displacement for the stiff and flexible configurations can be seen in Figure 4(a) and 4(b), respectively, for the angles of attack 0°, 6°, and 14°. The flexible configuration presented a wingtip displacement equals 90, 128, and 168 mm, for $\alpha = 0°$, 6° and 14°, respectively.

The identification of the wing displacement is a non-invasive technique and does not influence the wing response. However, improvements must be implemented to take into account the wing profile geometry during the post-processing of the images. For instance, for low angles of attack, the algorithm identifies as the upper and the lower bounds, the higher profile thickness, and the trailing edge, respectively. Notwithstanding, for higher angles, it identifies the tangent point formed by the camera line-of-sight with the profile and the trailing edge as upper and lower bounds. At last, for small angles of attack, the opposite occurs.

The inertial sensors embedded into the wing measured the wing torsion. The angle measurements for α = 0, 6 and 14 degrees can be seen in Table 1. The average values obtained are in agreement with the expected wing behavior. The location of the shear center leads to a wing washout when the wing is loaded. For the previous angles of attack, a washout of 1.00, 1.28, and 1.71 was observed, respectively. The significant deviations observed are considered to be mainly due to the model oscillations during the tests and the IMU signal conditioning. Authors consider that improvements in the signal conditioning algorithms can reduce the angle deviation. It is important to highlight that the sensors and cables weight, as well as their location, influence the wing response. Although these sensors can change the wing response, they do not interfere directly in the surrounding airflow. The values observed for IMU 5 (located closer to the wing root) show that the angle of attack set differs from the wing root one. Unconstrained 150 mm between the wing root and balance fixture can explain this difference.

4 Conclusions

The experimental investigation showed that different levels of airframe stiffness for a given wing planform and flow condition have significant effects on its aerodynamic lift and drag coefficients

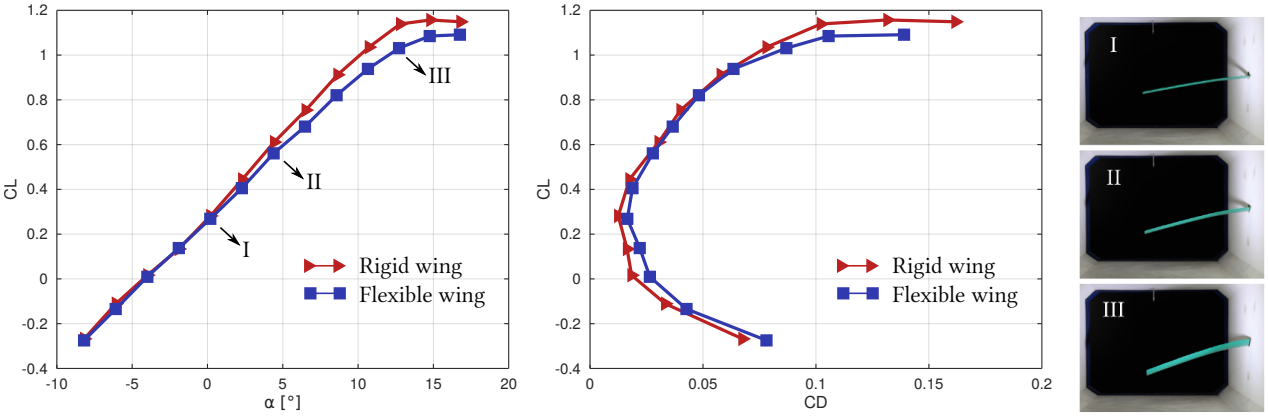

Fig. 3 Aerodynamic coefficients for rigid and flexible configurations: (a) lift coefficient vs. angle of attack and (b) drag vs. lift coefficient. (c) snapshots.

Table 1 Angles measurements from inertial sensors for flexible wing configuration.

$\alpha = 0°$		
IMU	θ_x [°]	θ_y [°]
1	9.32 ± 3.58	0.06 ± 6.2478
2	8.57 ± 3.00	-0.01 ± 4.0649
3	7.87 ± 3.31	0.41 ± 3.3693
4	6.45 ± 2.92	0.31 ± 6.2923
5	3.71 ± 2.97	1.06 ± 8.0587
$\alpha = 6°$		
IMU	θ_x [°]	θ_y [°]
1	13.2 ± 4.58	4.59 ± 7.75
2	12.3 ± 3.91	4.68 ± 1.30
3	11.3 ± 4.56	5.20 ± 2.35
4	9.52 ± 3.28	5.04 ± 4.98
5	5.36 ± 3.04	5.88 ± 6.50
$\alpha = 14°$		
IMU	θ_x [°]	θ_y [°]
1	16.5 ± 6.94	10.1 ± 5.82
2	15.6 ± 4.85	10.2 ± 2.76
3	14.3 ± 6.65	10.8 ± 2.24
4	12.3 ± 5.28	10.6 ± 5.16
5	7.01 ± 3.27	11.8 ± 6.82

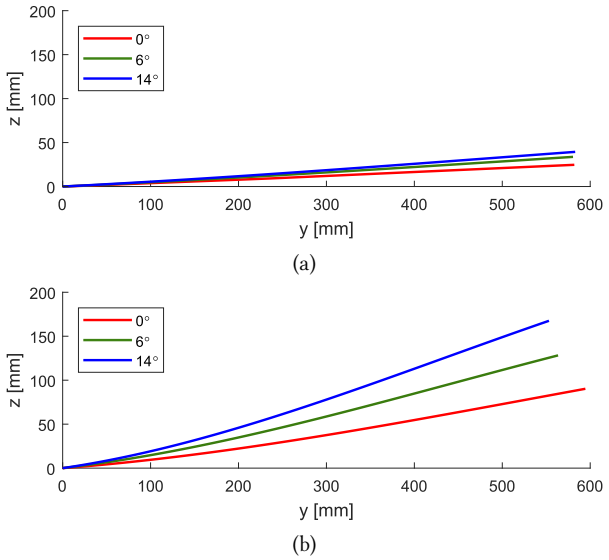

Fig. 4 Wing displacement in z-direction identified by image processing: (a) stiff and (b) flexible configurations.

and, for consequence, in some performance parameters. In general, the effect of flexibility for the presented wing was negative, showing that these effects must be taken into account in the aircraft design since its initial steps. However, investigations of the phenomenon for different wing planforms, stiffness and Reynolds numbers must and will be conducted in the continuity of the present work. Also, the usage of non-invasive measurement techniques for wing displacements

and twist showed to be very useful and reliable, although special care must be taken to avoid wing spar torsion between the wing model root and the balance. The results of the present article can be used in the validation of computational codes regarding the flexible wings modeling.

References

[1] Paur J. *Boeing 787 passes incredible wing flex test*. Available in: https://www.wired.com/2010/03/boeing-787-passes-incredible-wing-flex-test/, 2010. Acessed: 2017-07-28.

[2] Kingsley-Jones M. *Airbus A380 test wing breaks just below ultimate load target*. Available in: https://www.flightglobal.com/news/articles/airbus-a380-test-wing-breaks-just-below-ultimate-loa-204716/, 2006. Acessed: 2017-07-28.

[3] Tang D and Dowell E H. *Experimental and theoretical study of gust response for high-aspect-ratio wing*. AIAA Journal, 2002.

[4] Albertani R, Stanford B, Hubner J P and Ifju P G. *Aerodynamic coefficients and deformation measurements on flexible micro air vehicle wings*. Experimental Mechanics, 47(5):625-635, 2007.

[5] Hooker J R, Burner A W, Valla R. *Static Aeroelastic Analysis of transonic wind tunnel models using finite element methods*. AIAA Journal. 1997;(2243):254-261, 1997.

[6] Nguyen N T, Ting E, Chaparro D. *Nonlinear large deflection theory with modified aeroelastic lifting line aerodynamics for a high aspect ratio flexible wing*. 35th AIAA Applied Aerodynamics Conference. 2017;(June):1-26.

[7] Vassberg, J C, DeHaan, M C, Rivers, S M and Wahls, R A. *Development of a common research model for applied CFD validation studies*. AIAA Applied Aerodynamics Conference, AIAA 2008-6919, August 2008.

[8] Marchman III J F and Werme T D. *Clark-Y Airfoil Performance at low Reynolds numbers*. AIAA 22nd Aerospace Sciences Meeting, 1984.

[9] Pope A, Barlow J B and Rae Jr. W H. *Low-speed wind tunnel testing*. Third edition. John Willey and Sons. 1999; p. 713.

5 Contact Author Email Address

mailto: luis.pelegrineli@usp.br

Copyright Statement